Introduction

Production of a hydrocarbon reservoir changes the physical parameters of the subsurface. The extraction of oil and/or gas modifies the bulk modulus of the rocks and affects the geomechanics of the area. Stress changes induced by hydrocarbon production represent a key issue for constructing a geomechanical model of the reservoir. Monitoring these changes using remote sensing techniques is crucial for oil companies and contractors to be able to design wells, predict recovery, and mitigate hazards and risk (Lumley, 2001).

Seismic waves are sensitive to the elastic properties of the subsurface. The stress state of the subsurface is directly related to the propagation velocities of the waves. By repeated seismic surveys of the reservoir during the various production stages, we can track the changes in the physical paramenters in the subsurface and reconstruct the perturbation with respect to an initial model. The analysis exploits the sensitivity of the seismic waves to the elastic parameters of the subsurface. Inversion maps the changes in the waveforms, which are recorded at the surface, into a perturbation of the model parameters.

The analysis of time-lapse effects is usually performed in the time domain (Hatchell and Bourne, 2005) and assume small perturbations with respect to the background (baseline) model. The image domain is less sensitive to differences in the acquisition geometries and thus more robust against repeatability issues than the data domain. Shragge and Lumley (2012) propose a linearized inversion approach in the depth-domain based on the wave-equation migration velocity analysis algorithm developed by Sava and Biondi (2004). Shragge et al. (2012) apply to 4D seismic monitoring the methodology developed by Yang and Sava (2011), which uses the adjoint-state method (Fichtner et al., 2006) and removes the linearity assumptions. By operating directly in the depth domain and without linearity assumptions, the inversion can handle strong errors in the velocity model.

Wave-equation MVA (Sava and Biondi, 2004) and image-domain waveform tomography (Yang and Sava, 2011) require complete aperture to correctly construct the image perturbation that drives the tomographic procedure or to evaluate focusing in the subsurface. The requirements about the acquisition geometry can be relaxed using the approach proposed by (Yang and Sava, 2012), nonetheless, a large fixed-spread acquisition is necessary for resolution purposes. We advocate the use of local image correlations to measure the relative displacement between shot-migrated images (Hale, 2007) and use the inversion technique presented in (Perrone and Sava, 2012). Local image correlations allow us to estimate the errors in the velocity model shot by shot; the image-domain approach is robust against repeatability issues, such as errors in the shot and receiver positions, and the adjoint-state method allows us to implement a nonlinear inversion procedure.

Theory

Perrone and Sava (2012) restate the semblance principle considering locally coherent events in the image domain: the velocity model is correct when the images from different experiments show conformal features, that is, the dips of the reflectors in the two images are consistent. This criterium has been applied to migration velocity analysis using local image correlations to evaluate the relative movement of the two images with respect to the structural dips. We can use the same idea for 4D time-lapse seismic and compare the images obtained from the baseline and monitor survey. In this case, the baseline image represents our reference and we measure shifts of the monitor survery with respect to it. The shift is measured along the normal to the reflector (i.e., the dip direction).

We set an optimization problem by defining the objective function

$$\mathcal{J}(m) = \frac{1}{2} \| \sum_{\boldsymbol{\lambda}} \mathcal{P}(\mathbf{x}, \boldsymbol{\lambda})\, c(\mathbf{x}, \boldsymbol{\lambda}) \|^2_{\mathbf{x}}, \tag{1}$$

where $c(\mathbf{x}, \boldsymbol{\lambda}) = \int_{w(\mathbf{x})} R_{bsl}\left(\boldsymbol{\xi} - \frac{\boldsymbol{\lambda}}{2}\right) R_{mon}\left(\boldsymbol{\xi} + \frac{\boldsymbol{\lambda}}{2}\right) d\boldsymbol{\xi}$ is the local correlation of the baseline image R_{bsl} and the monitor image R_{mon} and $\mathcal{P}$ is a penalty operator that highlights features that are related to velocity errors. The correlations are computed in local seamless windows $w(\mathbf{x})$. The variable m denotes the model. When the velocity model is correct, the two images are perfectly aligned and the residual $\sum_{\boldsymbol{\lambda}} \mathcal{P}(\mathbf{x}, \boldsymbol{\lambda})\, c(\mathbf{x}, \boldsymbol{\lambda})$ (a proxy for the relative displacement) is minimum.

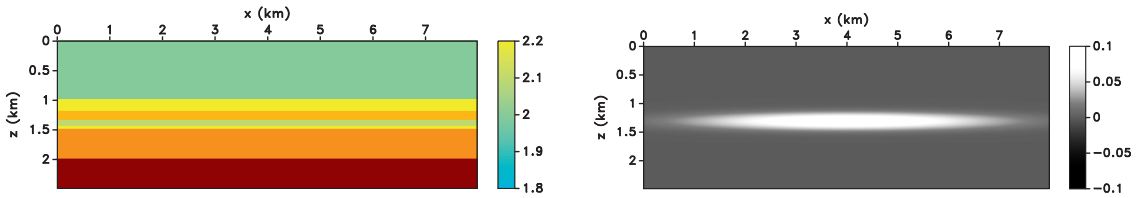

(a) (b)

Figure 1: (a) Velocity model used to generate the data and (b) the model perturbation.

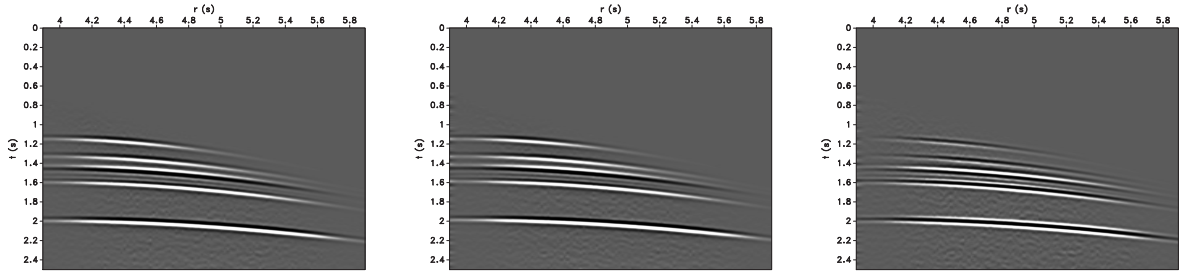

(a) (b) (c)

Figure 2: (a) Baseline data, (b) monitor data, and (c) data difference. Notice that because of the positioning error the events above the anomaly do not cancel.

We assume that the shifts between the migrated baseline and monitor survey are related to the errors in the velocity model. This is not necessarily true since changes in the stress conditions can cause compaction of the reservoir and lead to subsidence, that is a physical shifts of all the reflectors above the reservoir. Although subsidence up to 12 m due to hydrocarbon production has been observed and reported in the literature (for example in the Ekofisk field in the North Sea), shifts in the subsurface are usually negligible compared to the wavelegth of the seismic signal (few centimeters of the top and bottom of the reservoir (Steve Smith, personal communication)); it is thus safe to assume that the estimated shifts in the reflector positions are due to changes in the migration model.

The gradient of the objective function in equation 1 is computed using the adjoint-state method (Fichtner et al., 2006). The migrated images are defined as the correlation of source and receiver wavefield $u_s = u_s(\mathbf{x}, t)$ and $u_r = u_r(\mathbf{x}, t)$. The wavefields are computed by solving the wave equation

$$\mathcal{L}(m)\, u_s = f_s,\ \mathcal{L}(m)\, u_r = f_r, \tag{2}$$

where $\mathcal{L}(m)$ is the d'Alamber operator, $f_s = f_s(\mathbf{x}_s, t)$ and $f_r = f_r(\mathbf{x}_r, t)$ are the source and the seismic reflected data, respectively, and $\mathbf{x}_s$ and $\mathbf{x}_r$ indicate the source and receiver positions. The gradient of the objective function is

$$\nabla \mathcal{J} = \int (\ddot{u_s} a_s + \ddot{u_r} a_r) dt, \tag{3}$$

where the adjoint wavefields $a_s = a_s(\mathbf{x}, t)$ and $a_r = a_r(\mathbf{x}, t)$ are solutions of the wave-equations

$$\mathcal{L}^{\dagger}(m)\, a_s = g_s,\ \mathcal{L}^{\dagger}(m)\, a_r = g_r, \tag{4}$$

where $\mathcal{L}^{\dagger}$ is the adjoint of the d'Alamber operator, and the adjoint sources $g_s = g_s(\mathbf{x}, t) = \nabla_{u_s} \mathcal{J}$ and $g_r = g_r(\mathbf{x}, t) = \nabla_{u_r} \mathcal{J}$ are given by the Frechét derivatives of the objective function with respect to the background wavefields. The double dot indicates the second derivative with respect to time.

Synthetic Examples

We consider a simple synthetic example. We generate full-acoustic data using the velocity model in Figure 1(a) and a finite-difference algorithm. Figure 1(b) represents the perturbation in the velocity model

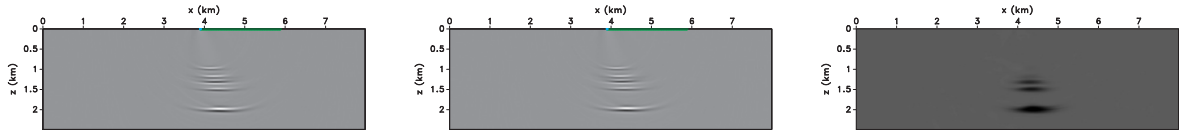

(a) (b) (c)

Figure 3: (a) Baseline image, (b) monitor image obtained using the baseline velocity model, and (c) relative shifts between the two images.

Figure 4: Estimated perturbation after 30 tomographic iterations.

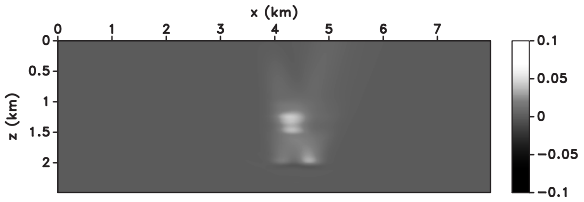

due to a change in the physical parameters in the medium. The anomaly is confined in a layer and may be caused by fluid substitution, stress changes due to compaction, etc. From an imaging perspective, these different physical phenomena translate into changes in the wave propagation velocities. The anomaly has a maximum amplitude of 0.1 km/s, which corresponds to about 5% of the background value. The vertical and horizontal sampling is 10 m and 20 m, respectively. The source function is a 15 Hz Ricker wavelet. Absorbing boundary conditions are applied so that no surface-related multiples are present in the data. We smooth the model vertically with a 10-sample triangular filter to obtain the baseline migration model.

Local image correlations allow us to measure velocity errors using a subset of the data (e.g. pairs of shot gathers); in particular, we can obtain model update by comparing single-shot migrated images (Perrone and Sava, 2012). We consider a single shot from the baseline and monitor survey. The source position in the baseline survey is at $x = 3.9$ km. We record data at 100 locations evenly spaced 20 m starting from the source position. We simulate a non-repeatable survey by randomly perturbing the positions of the source and receivers to model the monitor data. Figure 2 shows the baseline data, the monitor data, and their difference, respectively. Notice the first events in the data do not cancel because of the error in the shot position. From visual inspection, it is impossible to assess the quality of the baseline model for the monitor image, nonetheless the penalized local correlations highlight the shifts between the two images (Figure 3).We compute the gradient using the adjoint-state method and after 30 steepest-descent iterations, we obtain the estimated perturbation in Figure 4. Because of the limited aperture of the survey, only a portion of the anomaly is reconstructed. Nonetheless, we clearly see the anomaly building up in the correct layer.

Since we measure the displacement of the monitor with respect to the baseline image, we actually estimate the relative error between the monitor and baseline model. Figure 5 shows the baseline image, monitor image and their relative shift if the baseline velocity model is 5% faster than the model used in Figure 3. Both migrated images Figure 5(a) and 5(b) are defocused because of the bias in the baseline model. Nonetheless, the shifts only depend on the relative error between the baseline and monitor model

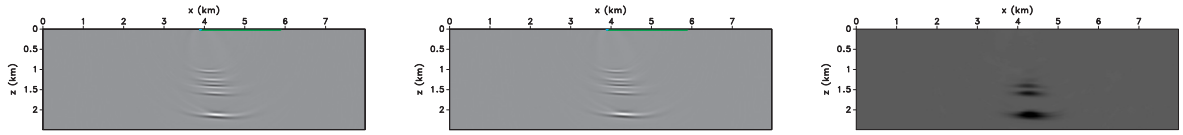

(a) (b) (c)

Figure 5: (a) Baseline image, (b) monitor image obtained using the baseline velocity model, (c) relative shifts between the two images. In this case, the migration velocity model is 5% faster than the correct model.

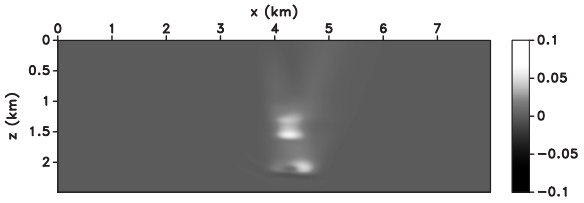

Figure 6: Estimated perturbation after 30 tomographic iterations with an incorrect baseline velocity model.

(Figure 5(c)).The result of the inversion is analogous, although slightly shifted in depth because of the bias in the baseline model (Figure 6).

Conclusions

Local correlations in the image domain allow us to assess the quality of the velocity model from a limited number of migrated images. In 4D seismic applications, we can quickly estimate perturbation in the migration model by comparing shot images from the baseline and monitor surveys. In the image domain, we measure the consistency and similarity of locally coherent events, like the local dip of the reflectors; these features are weakly sensitive to differences in the acquisition geometry and make our approach more robust against repeatability issues in the survey as compared to strategies in the data domain. The method is able to naturally recover the relative error in the velocity model and does not require separate velocity analysis steps for baseline and monitor survey in order to estimate the differences between the two models.

Acknowledgments

We would like to thank Joyti Behura for the interesting discussions about 4D time-lapse seismic and for pushing FP to look into it. This work was supported by the sponsors of the Center for Wave Phenomena at Colorado School of Mines. The reproducible numerical examples in this paper use the Madagascar open-source software package freely available from http://www.reproducibility.org. This research was supported in part by the Golden Energy Computing Organization at the Colorado School of Mines using resources acquired with financial assistance from the National Science Foundation and the National Renewable Energy Laboratory.

REFERENCES

Fichtner, A., H.-P. Bunge, and H.Igel, 2006, The adjoint method in seismology i. theory: Physics of the Earth and Planetary Interiors, 86–104.

Hale, D., 2007, A method for estimating apparent displacement vectors from time-lapse seismic data: Technical Report CWP-566, Center for Wave Phenomena, Colorado School of Mines.

Hatchell, P. J., and S. J. Bourne, 2005, Measuring reservoir compaction using time-lapse timeshifts: Presented at the 75th Ann. Internat. Mtg., Soc. of Expl. Geophys.

Lumley, D. E., 2001, Time-lapse seismic reservoir monitoring: Geophysics, **66**, 50–53.

Perrone, F., and P. Sava, 2012, Wavefield tomography based on local image correlation: Presented at the 74th Ann. Internat. Mtg., European Association of Geoscientists and Engineers.

Sava, P., and B. Biondi, 2004, Wave-equation migration velocity analysis. i. theory: Geophysical Prospecting, **52**, 593–606.

Shragge, J. C., and D. E. Lumley, 2012, 4d seismic wave-equation depth migration velocity analysis: Presented at the 74th Ann. Internat. Mtg., European Association of Geoscientists and Engineers.

Shragge, J. C., T. Yang, and P. Sava, 2012, Time-lapse image-domain velocity analysis using adjoint-state methods: Presented at the SEG Technical Program Expanded Abstracts, Soc. of Expl. Geophys.

Yang, T., and P. Sava, 2011, Image-domain waveform tomography with two-way wave-equation: Presented at the 81th Ann. Internat. Mtg., Soc. of Expl. Geophys.

———, 2012, Illumination compensation for image-domain wavefield tomography: Presented at the 74th Ann. Internat. Mtg., European Association of Geoscientists and Engineers.